Angular resolution at map level in the QUBIC instrument

M.M. Gamboa Lerena[1], C.G. Scóccola[1], P. Ade[2], J.G. Alberro[1], A. Almela[3], G. Amico[4], L.H. Arnaldi[5], D. Auguste[6], J. Aumont[7], S. Azzoni[8], S. Banfi[9,10], E.S. Battistelli[4,11], A. Baù[9,10], B. Bélier[12], D. Bennett[13], L. Bergé[14], J-Ph. Bernard[7], M. Bersanelli[15], M.A. Bigot-Sazy[16], N. Bleurvacq[16], J. Bonaparte[17], J. Bonis[6], A. Bottani[1], E. Bunn[18], D. Burke[13], D. Buzi[4], F. Cavaliere[15], P. Chanial[16], C. Chapron[16], R. Charlassier[16], A.C. Cobos Cerutti[3], F. Columbro[4,11], A. Coppolecchia[4,11], G. D'Alessandro[4,11], P. de Bernardis[4,11], G. De Gasperis[11,19], M. De Leo[4,29], M. De Petris[4,11], S. Dheilly[16], C. Duca[3], L. Dumoulin[14], A. Etchegoyen[3], A. Fasciszewski[17], L.P. Ferreyro[3], D. Fracchia[3], C. Franceschet[15], K. Ganga[16], B. García[3], M.E. García-Redondo[3], M. Gaspard[6], D. Gayer[13], M. Gervasi[9,10], M. Giard[7], V. Gilles[4], Y. Giraud-Heraud[16], M. Gómez Berisso[5], M. González[5], M. Gradziel[13], L. Grandsire[16], J-Ch. Hamilton[16], D. Harari[5], S. Henrot-Versillé[6], D.T. Hoang[16], F. Incardona[15], E. Jules[6], J. Kaplan[16], C. Kristukat[17], L. Lamagna[4,11], S. Loucatos[16], T. Louis[6], B. Maffei[20], S. Marnieros[14], W. Marty[7], S. Masi[4,11], A. Mattei[11], A. May[8], M. McCulloch[8], L. Mele[4,11], S. Melhuish[8], A. Mennella[15], L. Montier[7], L. Mousset[16], L.M. Mundo[1], J.A. Murphy[13], J.D. Murphy[13], F. Nati[9,10], E. Olivieri[14], C. Oriol[14], C. O'Sullivan[13], A. Paiella[4,11], F. Pajot[7], A. Passerini[9,10], H. Pastoriza[5], A. Pelosi[11], C. Perbost[16], M. Perciballi[11], F. Pezzotta[15], F. Piacentini[4,11], M. Piat[16], L. Piccirillo[8], G. Pisano[2], M. Platino[3], G. Polenta[21], D. Prêle[16], R. Puddu[22], D. Rambaud[7], P. Ringegni[1], G.E. Romero[23], M. Salatino[24], J.M. Salum[3], A. Schillaci[25], S. Scully[13,30], S. Spinelli[9], G. Stankowiak[16], M. Stolpovskiy[16], A.D. Supanitsky[3], A. Tartari[26], J.P. Thermeau[16], P. Timbie[27], M. Tomasi[15], S. Torchinsky[16], M. Tristram[6], G. Tucker[28], C. Tucker[2], D. Viganò[15], N. Vittorio[19], F. Voisin[16], F. Wicek[6], M. Zannoni[9,10] & A. Zullo[11]

[1] The list of affiliations is provided at the end of the article.

Contact / mgamboa@fcaglp.unlp.edu.ar

Resumen / Desde su descubrimiento en los años 1960, el fondo cósmico de microondas (CMB, por sus siglas en inglés) se ha convertido en una importante herramienta observacional para entender la física del universo temprano. El parámetro r, definido como la amplitud de las perturbaciones tensoriales relativas a las escalares, está acotado actualmente al rango $r < 0.056$. QUBIC es un instrumento terrestre diseñado para buscar señales muy débiles de los modos B en las anisotropías de la polarización a escalas angulares intermedias ($l \sim 30 - 200$). Para lograr este objetivo, QUBIC combina dos técnicas muy usadas en la comunidad CMB: interferometría y bolometría. En este trabajo calculamos la resolución angular de una simulación *end-to-end* con dos métodos independientes: *Fit* y *Sigma*. Concluimos que la reconstrucción que realiza el *software* es apropiada ya que la resolución medida con ambos métodos calibrados coincide con los valores teóricos de la resolución esperada.

Abstract / Since its discovery in the 1960s, the cosmic microwave background (CMB) radiation has become a very important observational tool to understand the physics of the early universe. The parameter r, defined as the relative amplitude of tensor to scalar perturbations, is currently constrained to the range $r < 0.056$. QUBIC is a ground-based instrument designed to search for very weak B-mode signals in polarization anisotropies at intermediate angular scales ($l \sim 30 - 200$). To achieve this goal, QUBIC combines two widely used techniques in the CMB community: interferometry and bolometry. In this work, we compute the angular resolution for an end-to-end simulation using two independent methods: *Fit* and *Sigma*. We conclude that the reconstruction performed by the software is appropriate since the resolution measured with both calibrated methods coincides with the theoretical value of the expected resolution.

Keywords / cosmic background radiation — early universe — instrumentation: interferometers

1. Introduction

The quest for the B-mode polarization of the cosmic microwave background (CMB) is one of the key goals of modern cosmology. Observing this mode appears to be the most powerful way to constrain Inflation models. The tensor-to-scalar ratio r, constrained via the primordial B modes in the CMB, is currently known to be $r < 0.056$, according to the Planck Collaboration (2018). However, detecting such a weak signal is an experimental challenge. In addition to high statistical sensitivity (requiring a large entrance aperture with the maximum number of sub-apertures, i.e. feedhorns, and a large focal plane well populated by detectors), future experiments will need excellent foreground removal and
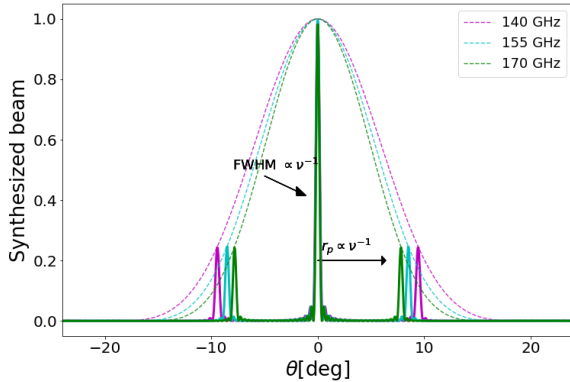
Figure 1: Radial cut of the normalized SB for 140 GHz (magenta), 155 GHz (cyan) and 170 GHz (green). The monochromatic SB changes for different frequencies. The distance r_p between the central and secondary peaks decreases with increasing frequency. The dashed line represents a Gaussian corresponding to the primary beam of a single horn for each frecuency.

unprecedented control of instrumental effects.

The Q&U Bolometric Interferometer for Cosmology (QUBIC), is a ground-based instrument that aims to measure the B-mode polarization anisotropy of the CMB (for details, see Mennella et al. 2019, García et al. 2019 , and references therein). It combines the sensitivity of transition edge sensors (TES) with the control of systematics allowed by the observation of interference fringe patterns (Bigot-Sazy et al. 2013) . A first module is planned to be installed at San Antonio de los Cobres, Salta, Argentina.

QUBIC will observe in two wide bands (25 %) centered at 150 GHz and 220 GHz. In this article, we focus on the 150 GHz focal plane. Since the synthesized beam (SB) is very well characterized, and thanks to the wide bandwidth, it is possible to reconstruct maps at many different subfrequencies within each frequency band. This spectral resolution defines QUBIC as a spectroimager. In Fig. 1 we see how the secondary peak locations, r_p, depend on frequency.

The aim of this work is to present a first approach to characterize the angular resolution of QUBIC instrument as modelled with the current software (pipeline). In Sec. 2., we explain the theoretical calculation of the SB. In Sec. 3., we show two independent methods developed to compute the resolution of reconstructed maps. We discuss our results for the measurements of the resolution with both methods in Sec. 4..

2. SB and theoretical resolution

The interference pattern is produced by the array of back-to-back horns and the optical combiner illuminating the focal plane. Depending on the number of open horns, n_h, the interference pattern will change due to the change in number of baselines.

The QUBIC pipeline simulates a full observation run, starting from an input simulated sky, x_ν, with

$\nu \in (130, 170)$ GHz. The number of input maps has to be large enough to simulate a wide-band observation into the focal plane. Hence, we use 15 input sub-maps to build the Time Ordered Data (TOD) (see Stolpovskiy 2015 for details),

$$y = H_\nu \, \boldsymbol{x}_\nu + \mathbf{n}, \tag{1}$$

where $\mathbf{n}$ is the instrumental noise and H_ν the acquisition operator. Once we have the TOD, we invert Eq. (1) to reconstruct the observed sky, through the map-making procedure, $\boldsymbol{x}_{\nu'} = (H^T N^{-1} H)^{-1} H^T N^{-1} y$, where N is the noise covariance matrix and ν' are the frequencies at reconstruction, different from the ones used to build the TOD.

As shown in Eq. (1), the TOD depends on the H_ν operator, which in turn depends on instrument configuration and scanning strategy. Once the instrumental configuration is set, the SB is well determined. By modelling the horn array as a regular square grid of P horns on a side spaced by a distance Δx, the SB can be analytically computed (see Battistelli et al. 2011 and Stolpovskiy 2015 for a detailed explanation) and it is straightforward to define the theoretical full width at half maximum (FWHM$_T$) as

$$\mathrm{FWHM_T} = \frac{\lambda}{P \Delta x}. \tag{2}$$

3. Fit and Sigma methods

In order to measure the angular resolution of the reconstructed map, we developed two independent methods, namely *Fit* and *Sigma*. The resolution is tested by applying the map-making procedure of QUBIC with a point source convolved at the corresponding frequency. This corresponds to a single non-zero pixel in a HEALPix[⋆] (Górski et al. 2005) projection map, which is afterwards smoothed using a Gaussian symmetric beam with FWHM given by

$$\mathrm{FWHM}(\nu) = \sqrt{8 \ln 2} \, \sigma(\nu). \tag{3}$$

The *Fit* method performs a normalized 2D asymmetric Gaussian fit to the maps, and as a result gives a two-axis mean dispersion of the fitted function. The model used to fit the location (x_c, y_c) and dispersion σ_x, σ_y is $M(x,y) = A \exp\left(-\frac{(x-x_c)^2}{2\sigma_x^2} - \frac{(y-y_c)^2}{2\sigma_y^2}\right)$, with an effective $\sigma = \sqrt{\sigma_x \sigma_y}$. For a nearly symmetric Gaussian, as in our case, we can approximate $\sigma = (\sigma_x + \sigma_y)/2$, to first order in the expansion of the square root. Finally, using Eq. (3), we compute the FWHM for that frequency.

The *Sigma* method computes the variance of a map, considering the map as a probability distribution function (PDF), $M^{PDF}(x,y)$. Since we are considering the map as a PDF, all of its values must be positive, and the function must be normalized ($\int M(x,y)dxdy = 1$). Reconstructed maps, in general, can have some negative values, so we need to set a cutoff in the map. All values below the given cutoff level are set to zero. Then, σ is mathematically defined as $\sigma^2 = \int x^2 m^{PDF}(x)\mathrm{d}x -$

[⋆] http://healpix.sourceforge.net

Table 1: Parameters used for calibration of the methods and the QUBIC pipeline. The parameter P is configured as if the Full Instrument (FI) was used. The HEALPIX parameters NSIDE and RESO are used for the projection of the maps.

Parameter	value
P (FI)	20
Δx	1.4 cm
ν	150 GHz (25 % bandwidth)
NSIDE	256
RESO	1.5

$\left(\int x m^{PDF}(x) \mathrm{d}x \right)^2$, where $m^{PDF}(x)$ is the marginalization of M over y-axis. Then, using Eq. (3) we compute the FWHM.

The parameters used for calibration and QUBIC simulations are summarized in Table 1. Eq. (2) with parameters values from Table 1 reads

$$\text{FWHM}_{\text{T}} \; [^\circ] = 61.34 \, \nu^{-1} \; [\text{GHz}]. \tag{4}$$

3.1. Calibration of the methods

Before measuring the angular resolution of the instrument, we need to calibrate the methods. The calibration consists in measuring the resolution of a point source smoothed at a given frequency with a given method m, FWHM^m and computing the difference with the theoretical resolution FWHM_{T}. The calibration was done using 50 equi-spaced values in the domain of $\nu \in (130, 170)$ GHz. For each frequency, a monte carlo simulation was carried out, and the results were averaged to obtain a measurement of the angular resolution.

The measured resolution is sensitive the HEALPIX RESO and NSIDE parameters, for the projection and resolution of the map, respectively. The parameter NSIDE is chosen in such a way that the pixel resolution does not interfere with QUBIC resolution. To avoid loss of resolution due to the HEALPIX projection, we set NSIDE = 256, corresponding to a pixel resolution of 13.7′. For QUBIC, that resolution corresponds to a frequency of 268 GHz, which is out of the frequency range of interest. With those considerations, we perform a Monte Carlo simulation to calibrate the methods. The average difference between FWHM_{T} and FWHM^{Fit} is $0.05^\circ \pm 0.01^\circ$, and between FWHM_{T} and $\text{FWHM}^{\text{Sigma}}$ is $0.03^\circ \pm 0.01^\circ$.

4. Results and discussion

After the methods are calibrated, we carry out a full simulation of an observation of a point source emitting in the broad band centered at 150 GHz. For the simulation, we use the QUBIC pipeline with the parameters in Table 1.

In Fig. 2 we show, in the upper figure, the measured values (light blue dots) of the FWHM computed with *Sigma* method and the calibrated (unbiased) values (blue dots). Dotted vertical lines represent the frequencies used to simulate the TOD. Each subpanel corresponds to an independent reconstruction using the same TOD. From the simulated TOD we can reconstruct a
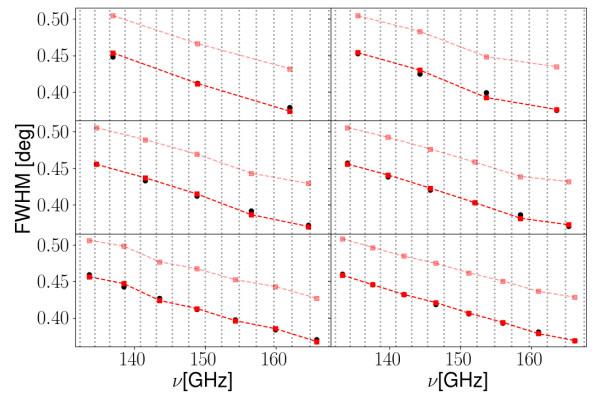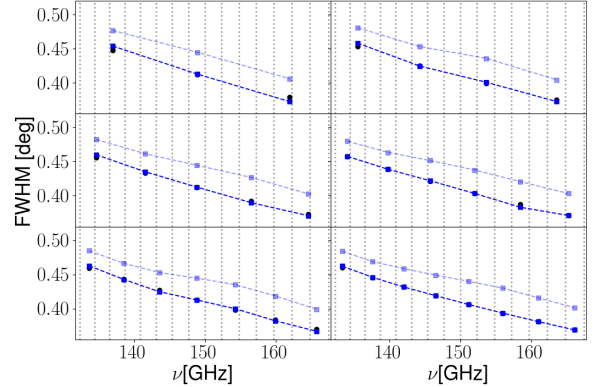

Figure 2: Theoretical values of the FWHM for each frequency (black dots). Light-color dots represent the measured values. Bold-color dots represent unbiased values using the calibration of each method. The upper (bottom) pannel shows measurements done with the *Sigma* (*Fit*) method. The dotted vertical lines represent the input frequency used to simulate a continuous input map to create the TOD.

number of maps N_{rec} inside the band considered. We reconstructed the maps for six different $N_{rec} = 3, 4, 5, 6, 7$ and 8, while $N = 15$ was used to build the TOD. The lower figure shows the same results but for the measurements using the *Fit* method. We include the theoretical values of the FWHM for each frequency in black dots.

The calibrated measured angular resolution for the output bands is acceptably unbiased: the maximum difference with respect to the theoretical value is up to 1.69% for the *Sigma* method, and up to 1.71 % for the *Fit* method.

5. Conclusions

In this article we show that the calibration for each of the methods defined to measure the FWHM is well understood, and we present the parameters that should be taken into account when doing QUBIC simulations.

The aim of this work was to present a first approach to characterize the angular resolution of QUBIC instrument. Another approach could be the scanning on point-like sources (i.e. planet or primary calibrators). In future works, we will advance on this direction.

The parameter r, relevant for inflationary models, is computed from the power spectrum of the anisotropies in temperature of the CMB polarization, i.e. Fourier transform of two point correlations function of the anisotropies in temperature. Motivated by this, we will next extend this study to the spectrum level. On the other hand, a computation of the ellipticity of the beam should be done, in order to have a more complete characterization of the beam. Furthermore, effects on angular resolution related to polarization issues should be also studied.

References

Battistelli E., et al., 2011, Astropart. Phys., 34, 705–716

Bigot-Sazy M.A., et al., 2013, A&A, 550, A59

García B., et al., 2019, Science Reviews from the end of the world (In press)

Górski K.M., et al., 2005, ApJ, 622, 759

Mennella A., et al., 2019, Universe, 5, 42

Planck Collaboration, 2018, arXiv e-prints, arXiv:1807.06209

Stolpovskiy M., 2015, Phd thesis, `http://theses.md.univ-paris-diderot.fr/STOLPOVSKIY_Mikhail_2_va_20161125.pdf`

List of affiliations

[1] *Facultad de Ciencias Astronómicas y Geofísicas, UNLP, Argentina*

[2] *Cardiff University, Cardiff, Reino Unido*

[3] *Instituto de Tecnologías en Detección y Astropartículas, CNEA–CONICET–UNSAM, Argentina*

[4] *Università di Roma, La Sapienza, Roma, Italia*

[5] *Centro Atómico Bariloche e Instituto Balseiro, CNEA, Argentina*

[6] *Laboratoire de l'Accélérateur Linéaire, Centre National de la Recherche Scientifique – Institut National de Physique Nucléaire et de Physique des Particules, Orsay, Francia*

[7] *Institut de Recherche en Astrophysique et Planétologie, Centre National de la Recherche Scientifique – Institut National des Sciences de l'Univers, Toulouse, Francia*

[8] *University of Manchester, Manchester, Reino Unido*

[9] *Università degli Studi di Milano-Bicocca, Milano, Italia*

[10] *Istituto Nazionale di Fisica Nucleare, Sezione di Milano Bicocca, Milano, Italia*

[11] *Istituto Nazionale di Fisica Nucleare, Sezione di Roma, Roma, Italia*

[12] *Centre de Nanosciences et de Nanotechnologies, Orsay, Francia*

[13] *National University of Irleland, Maynooth, Irlanda*

[14] *Centre de Spectrométrie Nucléaire et de Spectrométrie de Masse, Centre National de la Recherche Scientifique – Institut National de Physique Nucléaire et de Physique des Particules, Orsay, Francia*

[15] *University of Milan, Dept. of Physics, Milano, Italia*

[16] *Astroparticule et Cosmologie, Centre National de la Recherche Scientifique – Institut National de Physique Nucléaire et de Physique des Particules, Paris, Francia*

[17] *Comisión Nacional De Energia Atómica, Argentina*

[18] *Richmond University, Richmond, EE.UU.*

[19] *Università di Roma Tor Vergata, Roma, Italia*

[20] *Institut d'Astrophysique Spatiale, Centre National de la Recherche Scientifique – Institut National des Sciences de l'Univers, Orsay, Francia*

[21] *Agenzia Spaziale Italiana, Rome, Italia*

[22] *Instituto de Astrofísica, Pontificia Universidad Católica de Chile, Santiago, Chile*

[23] *Instituto Argentino de Radioastronomía, CONICET–CICPBA, Argentina*

[24] *Kavli Institute for Particle Astrophysics and Cosmology, Stanford, EE.UU.*

[25] *California Institute of Technology, Pasadena, EE.UU.*

[26] *Istituto Nazionale di Fisica Nucleare, Sezione di Pisa, Pisa, Italia*

[27] *University of Wisconsin, Madison, EE.UU.*

[28] *Brown University, Providence, EE.UU.*

[29] *Department of Physics, University of Surrey, Guildford, Reino Unido*

[30] *Institute of Technology Carlow, Carlow, Irlanda*